AFRL-ML-WP-TP-2007-402

A STUDY OF STRESS DISTRIBUTION IN LAYERED AND GRADIENT TRIBOLOGICAL COATINGS (PREPRINT)

Young Sup Kang, Shashi K. Sharma, Jeffrey H. Sanders, and Andrey A. Voevodin

NOVEMBER 2006

Approved for public release; distribution unlimited.

STINFO COPY

MATERIALS AND MANUFACTURING DIRECTORATE
AIR FORCE RESEARCH LABORATORY
AIR FORCE MATERIEL COMMAND
WRIGHT-PATTERSON AIR FORCE BASE, OH 45433-7750

NOTICE AND SIGNATURE PAGE

AFRL-ML-WP-TP-2007-402 HAS BEEN REVIEWED AND IS APPROVED FOR PUBLICATION IN ACCORDANCE WITH ASSIGNED DISTRIBUTION STATEMENT.

*//Signature//

ANDREY A. VOEVODIN, Program Manager
Nonstructural Materials Branch
Nonmetallic Materials Division

//Signature//

JEFFREY H. SANDERS, Chief
Nonstructural Materials Branch
Nonmetallic Materials Division

//Signature//

SHASHI K. SHARMA, Acting Deputy Chief
Nonmetallic Materials Division
Materials and Manufacturing Directorate

*Disseminated copies will show "//Signature//" stamped or typed above the signature blocks.

REPORT DOCUMENTATION PAGE

Form Approved
OMB No. 0704-0188

1. REPORT DATE *(DD-MM-YY)*	2. REPORT TYPE	3. DATES COVERED *(From - To)*
November 2006	Journal Article Preprint	

4. TITLE AND SUBTITLE
A STUDY OF STRESS DISTRIBUTION IN LAYERED AND GRADIENT TRIBOLOGICAL COATINGS (PREPRINT)

5a. CONTRACT NUMBER
F33615-03-D-5801

5b. GRANT NUMBER

5c. PROGRAM ELEMENT NUMBER
62102F

6. AUTHOR(S)
Young Sup Kang (Universal Technology Corporation)
Shashi K. Sharma, Jeffrey H. Sanders, and Andrey A. Voevodin (AFRL/MLBT)

5d. PROJECT NUMBER
4349

5e. TASK NUMBER
LO

5f. WORK UNIT NUMBER
VT

7. PERFORMING ORGANIZATION NAME(S) AND ADDRESS(ES)

Universal Technology Corporation
1270 N. Fairfield Road
Dayton, OH 45432

Nonstructural Materials Branch (AFRL/MLBT)
Nonmetallic Materials Division
Materials and Manufacturing Directorate
Air Force Research Laboratory, Air Force Materiel Command
Wright-Patterson Air Force Base, OH 45433-7750

8. PERFORMING ORGANIZATION REPORT NUMBER

9. SPONSORING/MONITORING AGENCY NAME(S) AND ADDRESS(ES)
Materials and Manufacturing Directorate
Air Force Research Laboratory
Air Force Materiel Command
Wright-Patterson AFB, OH 45433-7750

10. SPONSORING/MONITORING AGENCY ACRONYM(S)
AFRL-ML-WP

11. SPONSORING/MONITORING AGENCY REPORT NUMBER(S)
AFRL-ML-WP-TP-2007-402

12. DISTRIBUTION/AVAILABILITY STATEMENT
Approved for public release; distribution unlimited.

13. SUPPLEMENTARY NOTES
Journal article submitted to Tribological Transactions magazine.
The U.S. Government is joint author of this work and has the right to use, modify, reproduce, release, perform, display, or disclose the work.
PAO Case Number: AFRL/WS 06-2829, 11 Dec 2006. Paper contains color content.

14. ABSTRACT
A numerical model was used to determine the stress distribution in layered and gradient coatings. A parametric study was performed to investigate the effect of various critical parameters such as thickness, composition, applied load, material properties, and interfacial friction on the stress distribution in the layered and gradient coatings and the 440C steel substrate. Layered and gradient Ti/TiC coatings consisted of a titanium bond layer and titanium carbide (TiC) gradient layers. The $Ti_{1-x}C_x$ gradient coatings ($0 \leq x \leq 1$) were assumed as a series of perfectly bonded layers with unique material properties and layer thickness. The importance of the material, geometrical and mechanical effects on the magnitude and location of peak stresses were investigated. The results of this study can be used to optimize layered and gradient coating composition and thickness for the best tribological performance at specified contact loading conditions.

15. SUBJECT TERMS
Tribological coatings; gradient coatings; bonded layers

16. SECURITY CLASSIFICATION OF:			17. LIMITATION OF ABSTRACT:	18. NUMBER OF PAGES	19a. NAME OF RESPONSIBLE PERSON (Monitor)
a. REPORT	b. ABSTRACT	c. THIS PAGE			Andrey A. Voevodin
Unclassified	Unclassified	Unclassified	SAR	36	19b. TELEPHONE NUMBER *(Include Area Code)* N/A

Standard Form 298 (Rev. 8-98)
Prescribed by ANSI Std. Z39-18

Abstract

A numerical model was used to determine the stress distribution in layered and gradient coatings. A parametric study was performed to investigate the effect of various critical parameters such as thickness, composition, applied load, material properties, and interfacial friction on the stress distribution in the layered and gradient coatings and the 440C steel substrate. Layered and gradient Ti/TiC coatings consisted of a titanium bond layer and titanium carbide (TiC) gradient layers. The $Ti_{1-x}C_x$ gradient coatings ($0 \leq x \leq 1$) were assumed as a series of perfectly bonded layers with unique material properties and layer thickness. The importance of the material, geometrical and mechanical effects on the magnitude and location of peak stresses were investigated. The results of this study can be used to optimize layered and gradient coating composition and thickness for the best tribological performance at specified contact loading conditions.

Introduction

When two bodies are in contact with relative motion while supporting load, stress and deformation fields are generated below the contact surface. The service life of machine components is major concern to the manufacturers and it is greatly influenced by the friction and wear characteristics of the contacting surfaces. Tribological behavior of the mating surfaces can be significantly improved by depositing thin hard coatings on them. Thin layer coatings such as TiN, TiC, CrN, and TiCN deposited on the contacting surfaces have been developed for various applications to reduce the friction and wear of the engineering components that experience severe operating conditions. Recently, diamond-like carbon (DLC) coatings were recognized as the wear protective coatings since amorphous DLC materials have the unique combination of high hardness, low friction and low wear. Although DLC coatings have the superior friction and wear characteristics to the conventional thin layer coatings, DLC coatings deposited on the soft steel substrates have some disadvantages such as residual compressive stress and poor adhesion strength. Voevodin et al. (1995) showed that DLC coatings on the steel substrates have the application limitations such as contact pressure (below 1 GPa) and coating thickness (below 0.5 μm) in order to avoid the coating failure, i.e. brittle fracture and delamination, at the coating/substrate interfaces due to the significant material property differences. The limitations of DLC coatings were overcome by applying multilayer design concepts to the coating system. Voevodin et al. (1997a) developed the several design concepts for the architecture of multilayer coatings to improve the limitations of the DLC coatings. They suggested the functionally gradient (FG) Ti/TiC/DLC coatings increase the load support and adhesion of the DLC coatings while maintaining low friction at the contacting surfaces. In such coatings, the composition and hardness vary gradually from the substrate to DLC, avoiding drastic variations in material properties. In addition, Voevodin et al. (1997b) developed the optimized design of hard coatings using the multilayer and functionally gradient (FG) approach experimentally. They found that the design architecture provided the gradual increase of the hardness from the substrate to DLC coating and substantially increased the adhesion of DLC coating. Proper design of multilayer and functionally gradient (FG) coatings requires a through understanding of layer architecture, chemistry and mechanical properties. Also, to understand the failure mechanism of the coatings, the study of the stress distribution and its magnitude at the contact interface and inside the coating system is significantly important.

Since the early 1950s, most of the early works were focused to develop the mathematical formulations and analytical solutions for the plain strain contact problems such as the elastic deformation of the layered media. Meijers (1968) proposed mathematical formulations for the contact problem of a rigid cylinder pressed on an elastic layered media using asymptotic solutions. Satisfactory solution for all values of c/b (half width of contact area/layer thickness) and for Poisson' ratio between 0.0 and 0.5 was obtained for thin and thick layers. In 1970s, numerical analysis for the plain strain contact problems was performed by many researchers to avoid the mathematical complexity. Gupta and Walowit (1974) developed a mathematic formulation for the normal contact of layered elastic solids using Fourier transform approach of Airy stress function. Numerical solutions of contact pressure and size of contact zone for a wide range of layer

thickness were determined. Chiu and Hartnett (1983) solved three dimensional counterformal contact problems involving layered solids using the generalized Boussinesq solution. King and O'Sullivan (1987) developed a two dimensional quasi-static model to determine the stress field in layered elastic half-space under combined normal and sliding cylindrical contact. O'Sullivan and King (1988) extended the two dimensional model to the full three dimensional model to determine the subsurface stresses under the combined normal and sliding contact on a elastic half space with a layer for different material properties of layers and substrate system. Cole and Sayles (1992) developed a two dimensional numerical model for the contact of layered elastic bodies with real rough surfaces. They found that rough body layered contact has considerable influence on contact pressure behavior than smooth body layered contact. Also, Kuo and Keer (1992) developed a three dimensional model to consider a multilayered half space under combined normal and sliding contact by a spherical indenter using Hankel transforms. They discussed the stress components for various coating thicknesses. Polonsky and Keer (2000) applied the fast Fourier transform (FFT) technique with the multi-level multi-summation technique to the elastic layered contact problem. Chudoba et al. (2002) developed a novel methodology based on the combination of theoretical image loads method and indentation experiments for the evaluation of the response of coated substrates to mechanical contact. They showed that the effects of the addition of intermediate layer to the coating/substrate systems. Although many researchers developed the numerical models for the layered medium contact problems, their models were confined to the elastic contact behavior of the coating system.

As an alternative numerical approach, finite element analysis has been carried by a few researchers for the contact problem of layered surfaces. Komvopoulos (1988) developed a two dimensional finite element model to investigate the thin layer effects on elastic semi-infinite solid compressed by a rigid body and found the general solutions for the subsurface stress and deformation fields. Also, the parametric analysis of layer thickness relative to Hertzian contact width size, friction coefficient and stiffness of layer were performed. Komvopoulos (1989) extended the elastic layered media finite element model to the elastic-plastic contact problem of TiN/Ti coating system. The critical parameters such as layer thickness, material properties of layer and substrate materials and indentation depth on the threshold of plasticity of the elastic-plastic layered media indented by a rigid cylinder were examined. He found that the coating thickness plays an important role on the initiation and propagation of plastic zone and developed a deformation map for TiN/Ti coating systems. Bhattacharya and Nix (1988) developed an elastic and plastic model to study the deformation associated with indentation of the thin film/substrate system using the finite element method and found the effects of the elastic and plastic properties of the materials on the hardness of the film/substrate system. Also the elastic compliance of the film/substrate system was determined as a function of the indentation depth from the load-displacement curve. Sun et al. (1995) developed an elastic-plastic axisymmetric finite element model to investigate the effects of important parameters such as thickness of coatings and material properties of substrates on the various TiN coating/substrate systems. They found that substrate strength and layer thickness play significant roles on the load capacity of the systems, development of plastic zone, and subsequent coating failure. Kral and Komvopoulos (1997) developed a

three dimensional finite element model to determine the subsurface stress and strain fields due to sliding contact on an elastic-plastic layered medium. They found the effects of layer material properties, friction coefficient, and applied load on the stresses in the layer and the substrate. Ye and Komvopoulos (2003) developed the three dimensional finite element model to investigate the effect of residual stress in the layered media due to normal and sliding loading and unloading conditions. They showed the optimum residual stress in the layer is a function of loading type and friction coefficient. Although many analytical and numerical works have been performed to observe the various coating systems, no previous work has attempted to observe the layered and gradient Ti/TiC coating system in spite of the recognition of the friction and wear performance of layered and gradient coating system (Voevodin et al., 1997b).

Therefore, it is of significant importance to analyze the stress distribution of the layered and gradient Ti/TiC coatings and substrate through the development of a finite element model to identify the critical parameters that constrain the deformation and subsurface stresses of coating system caused by normal contact conditions. In the present study, a three dimensional finite element model has been developed to simulate the elastic plastic indentation process of the layered and gradient Ti/TiC coating system in order to understand the mechanisms involved in tribological contacts for a wide range of material properties, coating thickness, composition, applied load, and friction using ABAQUS. Further, the study is to provide the design guideline for high load and adhesion applications.

Description of the Layered and Gradient Ti/TiC Coating System

Interfaces between layers are prime locations for coating failure since considerably different mechanical properties between the layers exist. Therefore, multilayer coatings with gradually changing composition (functionally gradient) are highly desirable to avoid the drastic changes of mechanical properties. Figure 1 shows the typical layered and gradient Ti/TiC/DLC coating displaying the compositional variation of the Ti/TiC/DLC coating deposited on the top of the 440C steel substrate (Voevodin, 1997b). Figure 2 depicts the indentation on the multilayered and gradient Ti/TiC coatings deposited on the semi-infinite medium with a rigid spherical indenter used for this study. Each coating surface is assumed to be smooth. The multilayered and gradient Ti/TiC coatings are assumed to be a series of perfectly bonded layers with unique material properties and layer thickness although the gradient coatings don't have distinct layers in reality, that is, they normally have continuous gradual change of Ti and C composition. The α-Ti layer is deposited on the 440C stainless steel substrate as a bond layer in order to enhance the adhesion between the substrate and TiC coatings. Then coatings from $Ti_{.90}C_{.10}$ to $Ti_{.30}C_{.70}$ with variational Ti/C composition are continuously deposited on the top of the bond layer. Figure 3 illustrates the schematic of functionally gradient (FG) Ti/TiC coating design. On the top of the 440C stainless steel substrate, α-Ti is added as a bond layer with 50nm thickness to improve the adhesion between the substrate and the $Ti_{.90}C_{.10}$ layer. On the top of the α-Ti layer, $Ti_{.90}C_{.10}$ is deposited with 50 nm thickness. As the TiC composition changes, the gradient coating is generated. Each layer has its unique material properties such as hardness, elastic modulus, and Poisson's ratio. Specific thickness for each layer is used for this application. Figure 3 consists of the material property values used for this present study. The detail for TiC gradient coating procedure

is well described in Voevodin et al. (1997b). Table 1 contains the contact conditions such as normal loads, coefficients of friction, thicknesses of $Ti_{.30}C_{.70}$ layer, indenter radius, and bond layers used in this analysis.

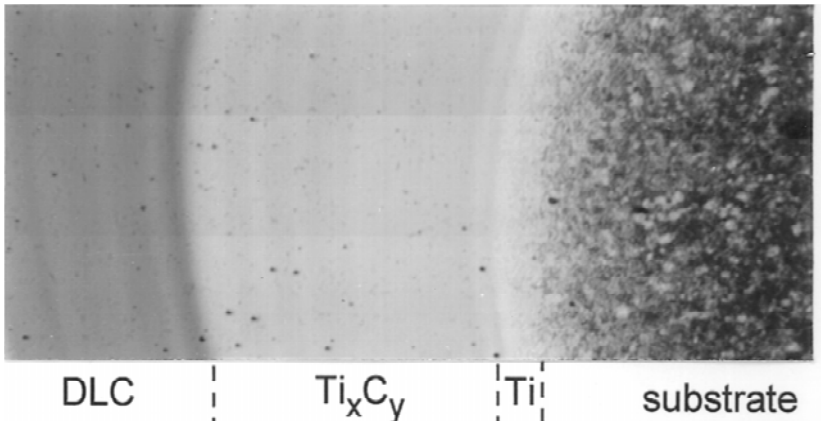

Figure 1. Typical layered and functionally gradient Ti/TiC/DLC coating deposited on 440C steel

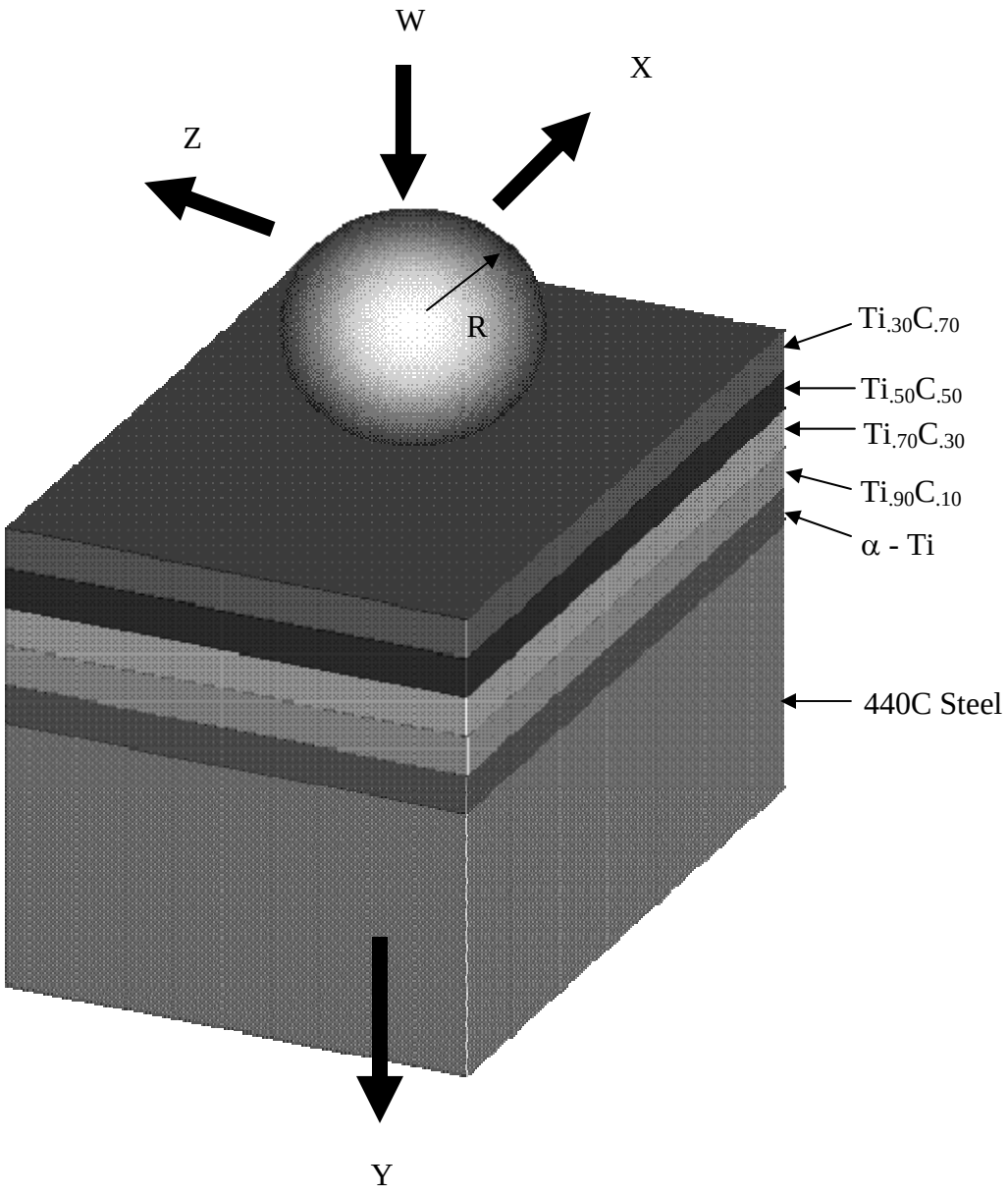

Figure 2. Schematic of indentation with a rigid spherical indenter on multilayered semi-infinite medium

Material	Hardness	Elastic Modulus	Thickness	Poisson's Ratio
$Ti_{.30}C_{.70}$	29 GPa	370 GPa	100 ~ 1000 nm	0.20
$Ti_{.50}C_{.50}$	20 GPa	290 GPa	100 nm	0.20
$Ti_{.70}C_{.30}$	14 GPa	230 GPa	100 nm	0.25
$Ti_{.90}C_{.10}$	6 GPa	150 GPa	50 nm	0.25
α-Ti	4 GPa	140 GPa	50 nm	0.25
440C steel	11 GPa	220 GPa		0.30

Figure 3. Schematic of functionally gradient Ti/TiC coating design with compositional and mechanical properties variation

ABAQUS Finite Element Model

The contact problem described in Figure 2 can be modeled with the finite element mesh shown in Figure 4. The finite element model is to analyze contact stress distribution in layered and gradient Ti/TiC coatings generated by a rigid spherical indenter. The commercial finite element software package ABAQUS™/Standard was used to model the layered and gradient Ti/TiC coatings under the plane-strain assumption. Due to the symmetry of the system, only a quarter of the computational domain was modeled. To reduce the computing time, the outer portion of computational domain was modeled as infinite body using infinite elements. In addition, very fine mesh was used for the gradient coatings adjacent to the coatings/rigid indenter interface near the contact zone in order to determine the stress distribution and deformation field accurately. Relatively coarse mesh was used for the region where is far away from the contact zone to reduced the computing time. Nearly 30,000 nodes and elements were used to model the entire system. Two types of elements, eight-node linear brick reduced integration element (C3D8R) and eight-node linear one-way infinite element (CIN3D8), were used for the coatings and semi-infinite medium. The coatings were modeled by assigning different material properties for the elements. The rigid spherical indenter is represented by a rigid spherical body with a radius, 0.2 μm.

Applied Normal Load (W)	4.4×10-4 ~ 0.15 (N)
Coefficient of Friction (μ)	0.0 ~ 0.6
Thickness of Ti.30C.70 (t)	100 ~ 1000 (nm)
Radius of Indenter (R)	0.0002 (m)
Bond Layers	α-Ti, Ti Alloy, Chromium

Table 1. Contact conditions

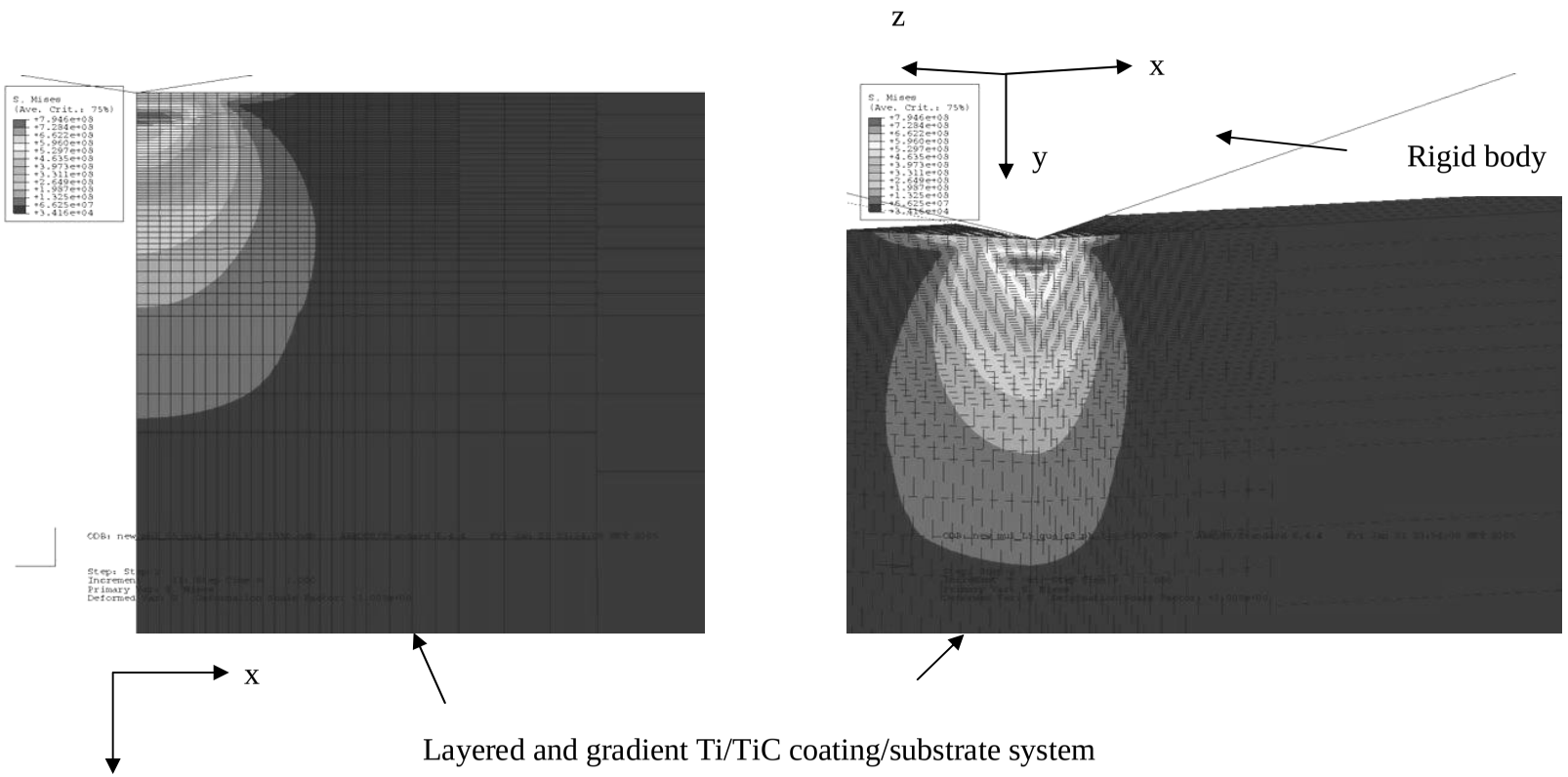

Figure 4. Schematic of three dimensional finite element model

Coulomb friction was used to model the contact between the top coating surface and the rigid indenter. Due to the perfect bonding assumptions, the continuous displacement at the coating interfaces and coating/substrate interface is applied. Since the strain hardening is not considered, elastic perfectly plastic stress-strain relationships were used for the gradient coatings and substrate. The onset of plastic yield begins by the von Mises yield criterion for the isotropic materials. Figure 4 illustrates the side and perspective view of the finite element model developed for this study. Figure 4 demonstrates the von Mises stress inside the coatings and substrate generated by a rigid spherical indenter on the plane of symmetry, x-y plane and x-y and y-z planes, respectively. The computation was performed using a workstation that consists of 9 dual-processor 900 MHZ Itanium2's with 2 Gigs of RAM each. Please note that the residual compressive stresses associated with the process of deposition are negligible because the layered and gradient coating thickness is a few micros.

Results and Discussion

In order to validate the three dimensional finite element model developed for this study, the elastic Hertzian point contact between the 440C stainless steel substrate and the rigid spherical indenter was performed. Figure 5 (a) shows the normalized Hertzian point contact pressure distribution generated by a rigid spherical indenter with the coefficient of friction, $\mu = 0.0$. Please note that the full contact pressure distribution was generated using the symmetry of the problem although a quarter of the computational domain was modeled. The magnitude of maximum Hertzian pressure is 1.0 GPa under a normal load, W = 0.0035 N. Figure 5 (b) depicts the contact pressure distributions at the center of the contact along the axis of symmetry obtained by finite element and analytical solutions for maximum Hertzian contact pressure, 1.0 GPa and 1.5 GPa, respectively. The discrepancy between the finite element and analytical results at the contact edge is due to the node discretization size of the contact elements. The results indicate that there is good agreement between the finite element and analytical solutions.

Please note that the full von Mises stress distribution on the plane of symmetry was plotted due to the symmetry of the problem. Von Mises stress is taken into account to analyze and predict the failure in the contact problems. Figure 6 represents the von Mises stress distributions generated by a rigid spherical indenter inside the 440C stainless steel substrate on the vertical plane of symmetry, i.e., x-y plane for a normal load W = 0.0035N and μ =0.0. Figures 6(a) depicts the perspective view of normalized von Mises stress at the center of the contact on the vertical plane of symmetry. This figure displays the smooth variation of von Mises stress along the depth direction, Y, as well as along the surface direction, X. The calculated maximum von Mises stress is 0.635 P_h located approximately at Y = 0.5 below the surface. Figure 6(b) illustrates the contour of the von Mises stress distribution presented in Figure 6(a).

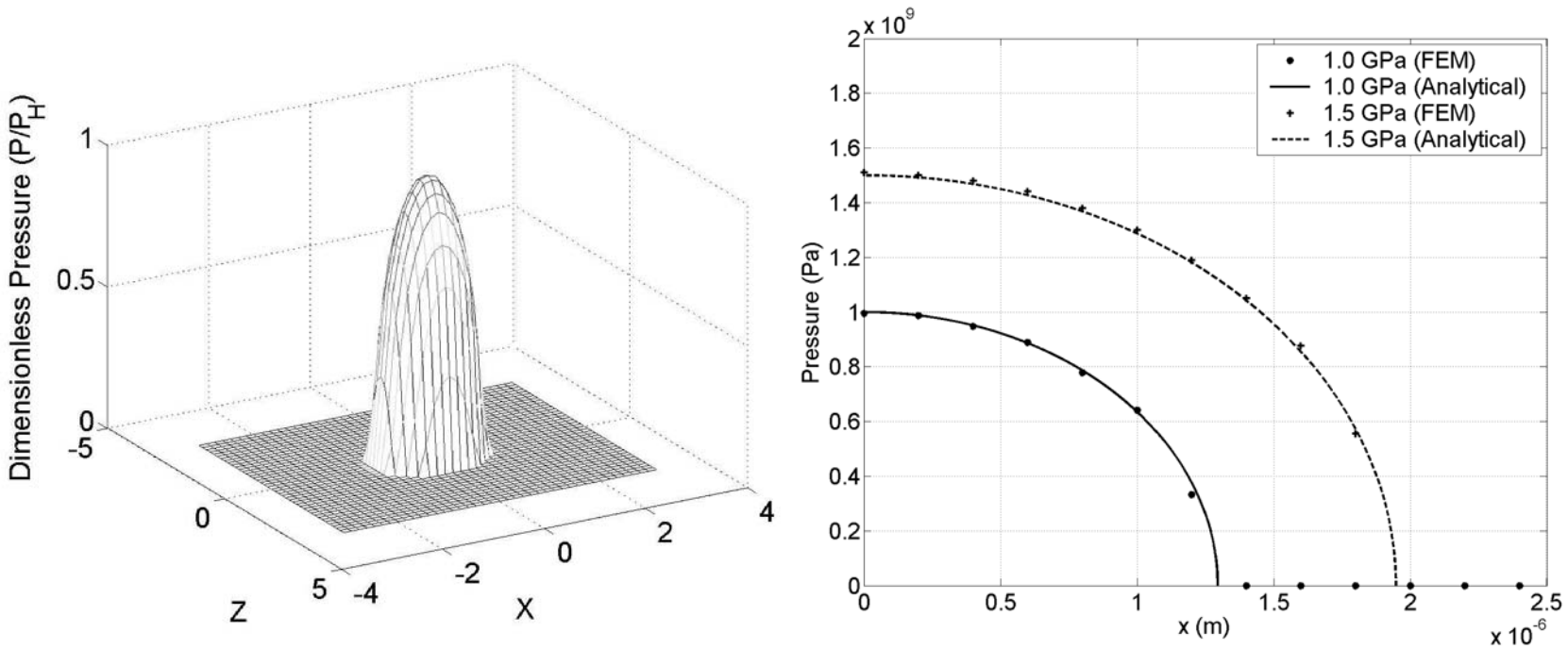

(a) (b)

Figure 5. Hertzian contact pressure distribution on semi-infinite medium indented by a rigid spherical indenter; (a) normalized contact pressure distribution by finite element solution for W = 0.0035 N and (b) contact pressure distributions at the center of contact along the plane of symmetry obtained by finite element and analytical solutions

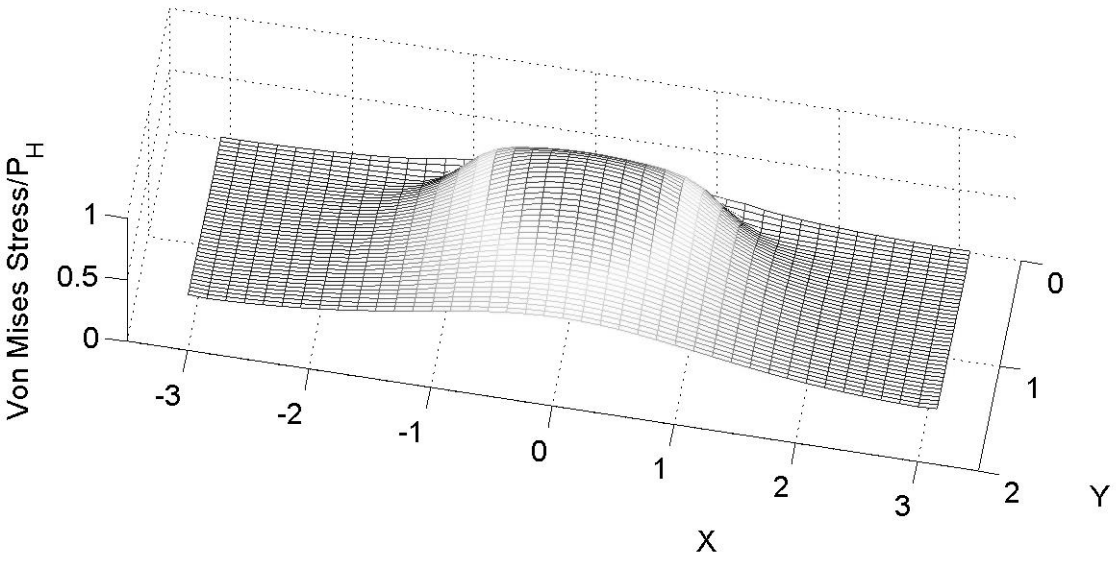

(a)

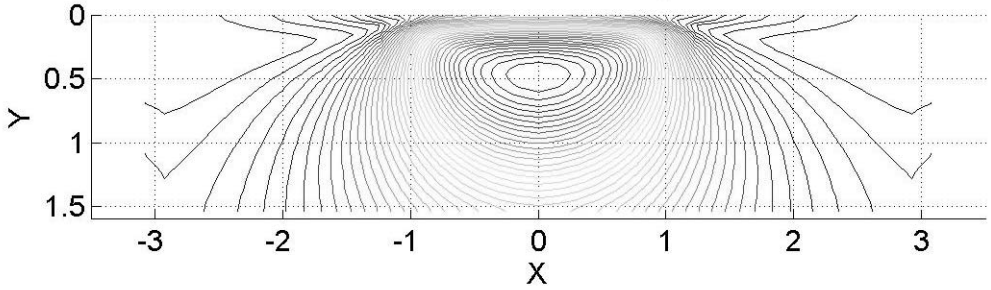

(b)

Figure 6. Von Mises stress distribution in semi-infinite medium indented by a rigid spherical indenter for normal load, W = 0.0035 N (μ = 0.0); (a) perspective view of normalized von Mises stress on the plane of symmetry and (b) contour of normalized von Mises stress on the plane of symmetry

Figure 7 demonstrates stress component profile variations below the surface at the center of the contact along the axis of depth for W = 0.0035 N and μ =0.0. Various lines are generated by the finite element solutions. Dots are generated by the analytical solutions for the same contact conditions. σ_x decreases rapidly as the depth increases. Due to the symmetry, σ_z has the same values with σ_x along the depth direction. σ_y has the maximum value, 1, at the surface and deceases gradually as the depth increases. σ_{mises} has the maximum value of 0.635 P_h located approximately at Y = 0.5 on the depth axis. In general, the good agreement for stress distribution between the finite element and analytical solutions was achieved at the various depths below the contact surface.

Figure 8 shows the stress component profile variations below the surface at the center of the contact along the axis of depth for W =0.0035 N and μ =0.0. The stress components such as σ_x, σ_y, σ_z, and σ_{mises} are displayed. The diagram depicts the layered and gradient Ti/TiC coating system with 350 nm $Ti_{.30}C_{.70}$ layer thickness. The stress component profiles display the discontinuities occurring at the interfaces due to the material property differences. Fundamentally, the layers behave as beams bonded to the substrate. The maximum von Mises stress occurs at the $Ti_{.50}C_{.50}$ and $Ti_{.70}C_{.30}$ interface. The von Mises stress difference at the interfaces is not exceeding 0.1 GPa. If more distinct layers, e.g. $Ti_{.85}C_{.15}$, $Ti_{.75}C_{.25}$, and $Ti_{.65}C_{.35}$, are used, the stress component profiles would become smoother. σ_x and σ_z is more influenced by the layered and gradient coatings while σ_y is less influenced. The magnitude and location of maximum von Mises stress can be altered significantly when the different design of layered and gradient coating system is used.

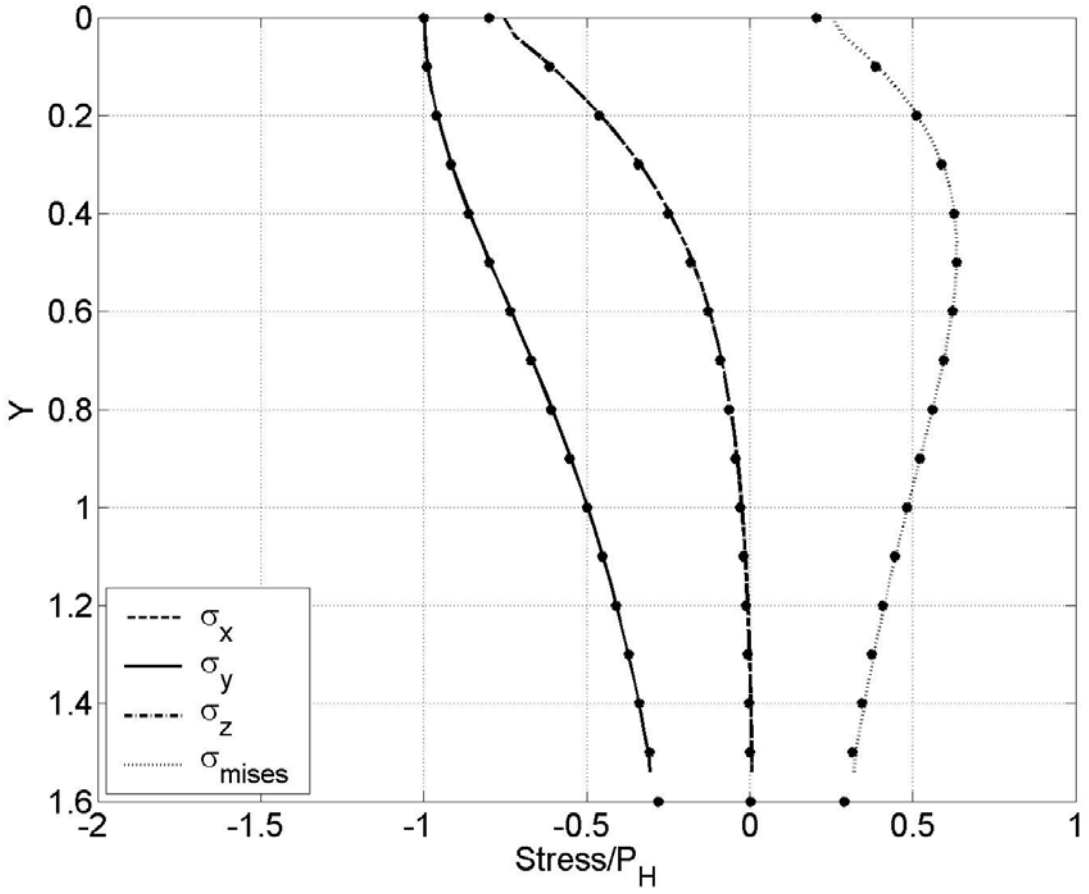

Figure 7. Analytical and finite element solutions of normalized stresses in the semi-infinite medium due to the normal load at the surface ($\mu = 0$)

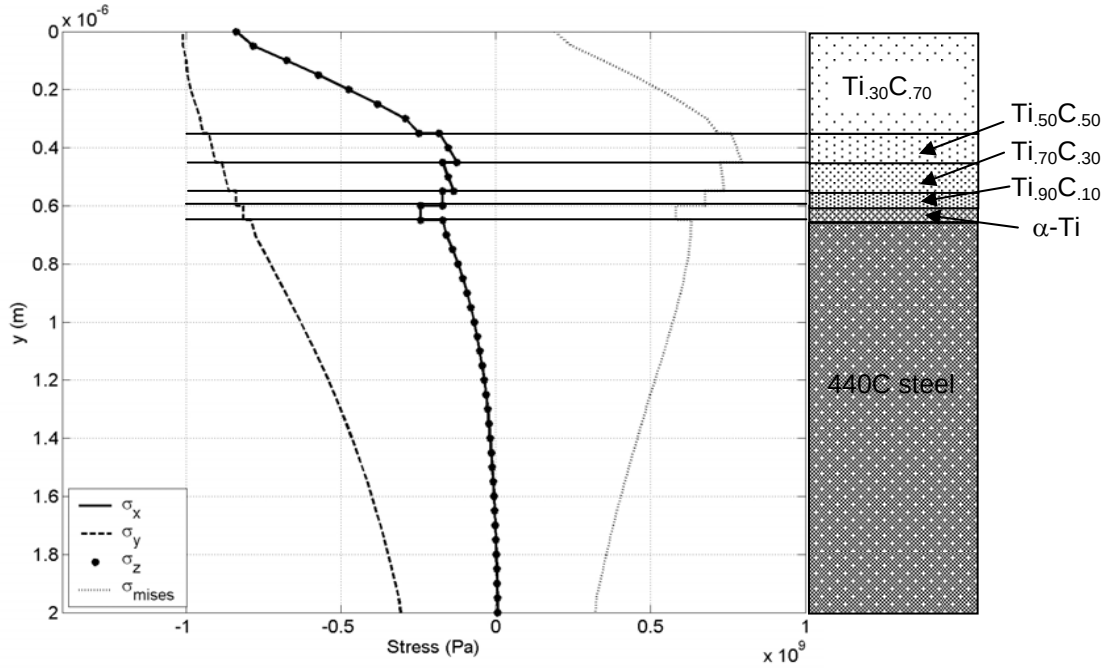

Figure 8. Analytical and finite element solutions of the stresses in a layered and gradient coating system due to normal load at the surface ($\mu = 0.0$)

Figure 9 represents the von Mises stress distribution of the layered and gradient Ti/TiC coating system on the plane of symmetry for the normal loading contact conditions with 350nm $Ti_{.30}C_{.70}$ layer thickness, W = 0.0035 N and μ =0.0. Figure 9(a) shows the perspective view of the von Mises stress generated by a rigid spherical indenter on the plane of symmetry. Instead of having smooth von Mises stress distribution inside the layered and gradient Ti/TiC coatings, discontinuous stress distribution at the layered and gradient coating interfaces exists due to the material property differences. Overall shape of von Mises stress distribution is similar to the one without the layered and gradient Ti/TiC coating. The calculated maximum von Mises stress is 795 MPa located at $Ti_{.50}C_{.50}$ and $Ti_{.70}C_{.30}$ interface along the depth direction below the surface. Figure 9(b) demonstrates the contour of the von Mises stress distribution presented in Figure 9(a).

Figure 10 shows the effect of coating design on von Mises stress for the normal load, W = 0.0035 N and μ= 0.0. Figure 10 illustrates the von Mises stress distribution comparison between a 700 nm $Ti_{.30}C_{.70}$ layer coating on 440C steel substrate and a 700 nm layered and gradient Ti/TiC coating on 440C steel substrate. Please note that the von Mises stress distributions are obtained at the center of the contact along the axis of depth below the contact surface. The magnitude of von Mises stresses occurred inside the $Ti_{.70}C_{.30}$, $Ti_{.90}C_{.10}$ and α-Ti coatings are smaller than the one of the monolayer coating because of the low moduli of elasticity for $Ti_{.70}C_{.30}$, $Ti_{.90}C_{.10}$ and α-Ti coatings. Monolayer coating depicts the sharp von Mises stress discontinuity occurring at the interface due to the high

modulus difference of film and substrate. However, the layered and gradient Ti/TiC coating represents the gradual stepped von Mises stress changes. While the monolayer coating has the maximum von Mises stress at the $Ti_{.30}C_{.70}$ and substrate interface, the layered and gradient Ti/TiC coating has its maximum von Mises stress at the $Ti_{.50}C_{.50}/Ti_{.70}C_{.30}$ interface. The magnitude of maximum von Mises stress decreases from 0.909 GPa to 0.818 GPa when the monolayer coating is replaced by the layered and gradient Ti/TiC coating. Therefore, the layered and gradient coating is more beneficial than monolayer coating since it reduces the magnitude of maximum von Mises stress in the coating system. In addition, it results in lower magnitude differences of von Mises stress at the interfaces.

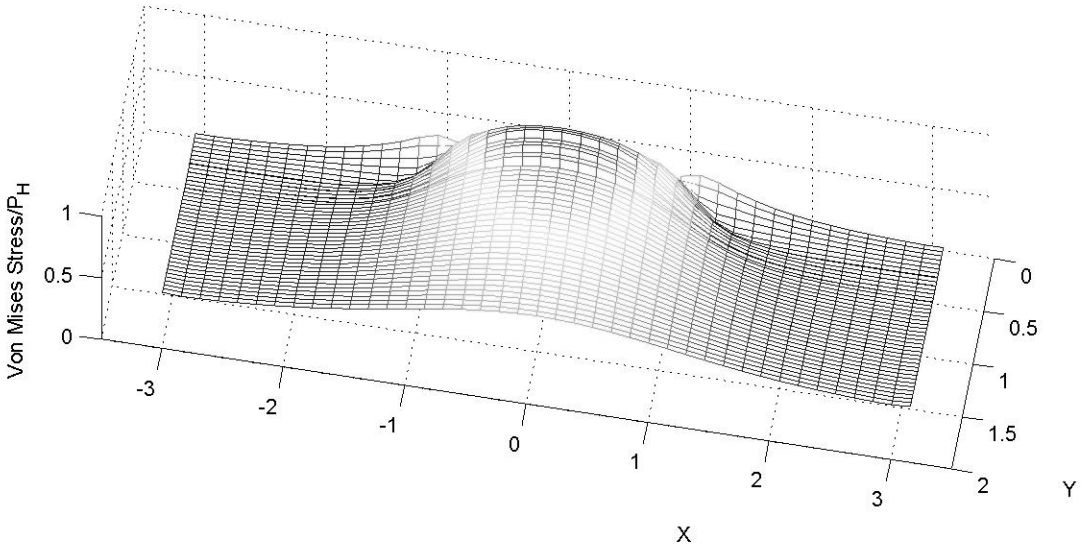

(a)

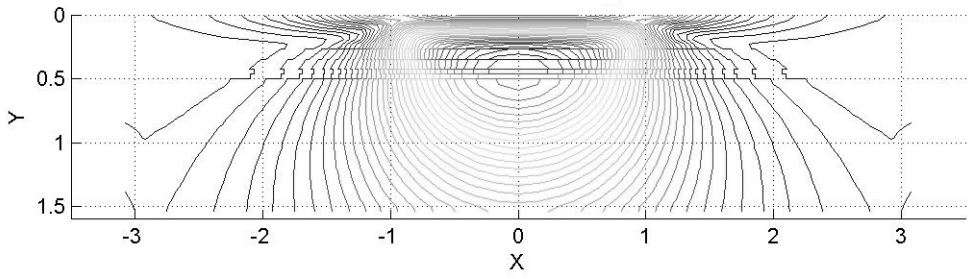

(b)

Figure 9. Von Mises stress distribution in layered and gradient Ti/TiC coating system indented by a rigid spherical indenter for indentation load, W = 0.0035 N (μ = 0.0); (a) perspective view of normalized von Mises stress on the plane of symmetry and (b) contour of normalized von Mises stress on the plane of symmetry

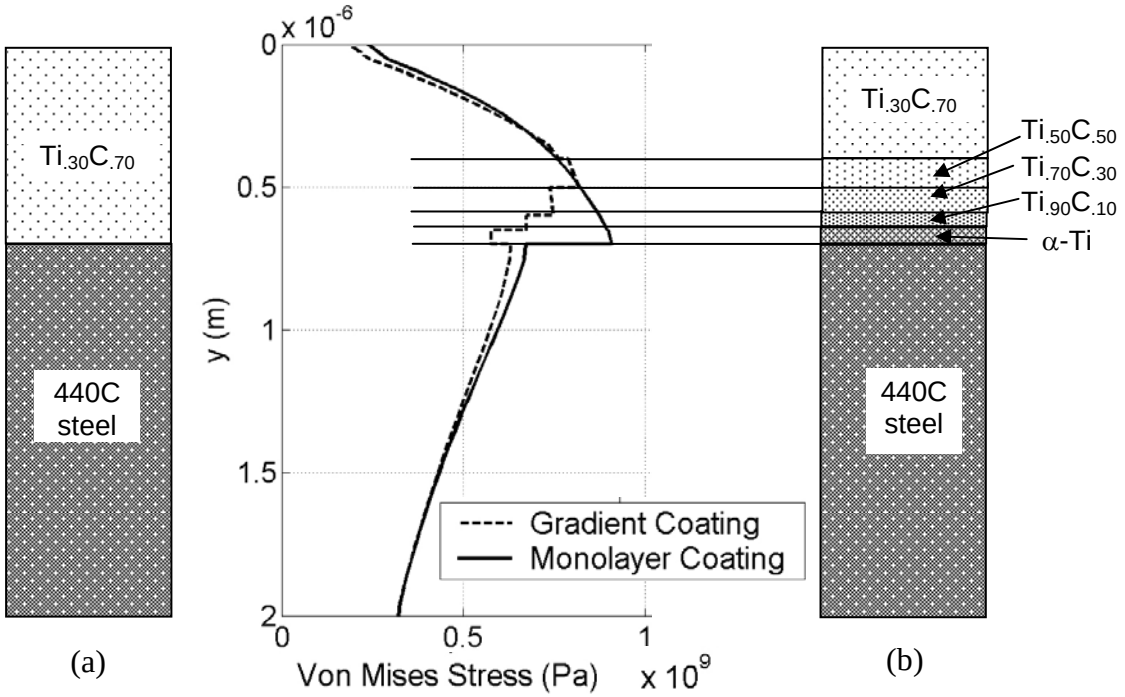

Figure 10. Effect of coating design on von Mises stress in (a) monolayer coating system and (b) layered and gradient coating system for normal load, W = 0.0035 N (μ = 0.0)

In order to represent the spatial distribution of von Mises stress in the layered and gradient Ti/TiC coating system, the results from the FEA model are presented. Figure 11 shows contours of von Mises stress in the layered and gradient Ti/TiC coating system indented by a rigid spherical indenter on the plane of symmetry, x - y plane. Figure 11 illustrates that the von Mises stress fields below the surface vary as the load increase from W = 4.4×10^{-4} N through 0.0283 N with μ = 0.0. Please note that the maximum von Mises stress always occurs at certain depth along the axis of depth below the center of the contact due to the symmetry of the problem. Figure 11(a) is the contour of von Mises stress for a normal load, W = 4.4×10^{-4} N. The maximum von Mises stress occurs inside the $Ti_{.30}C_{.70}$ coating with the magnitude of 415.7 MPa. With the relatively light normal load, W = 4.4×10^{-4} N, only shallow indentation depth occurs and shows the elastic behavior of the coating/substrate system. Figure 11(b) is the contour of von Mises stress for a normal load, W = 0.0035 N. The maximum von Mises stress occurs inside the $Ti_{.50}C_{.50}$ coating with the magnitude of 794.6 MPa. Figure 11(c) is the contour of von Mises stress for a normal load, W = 0.0119 N. The maximum von Mises stress occurs inside the $Ti_{.50}C_{.50}$ coating with the magnitude of 1.087 GPa. Figure 11(d) is the contour of von Mises stress for a normal load, W = 0.0283 N. The maximum von Mises stress occurs inside the substrate with the magnitude of 1.394 GPa. In general, as the applied normal load increases, the location of maximum von Mises stress moves from inside the layered and gradient Ti/TiC coatings to substrate. Also, as load increases, wider half Hertzian contact width and higher von Mises stress are generated. Due to the material

discontinuities inside the layered and gradient Ti/TiC coatings, there is discontinuous stress distribution at the interfaces below the contact surface.

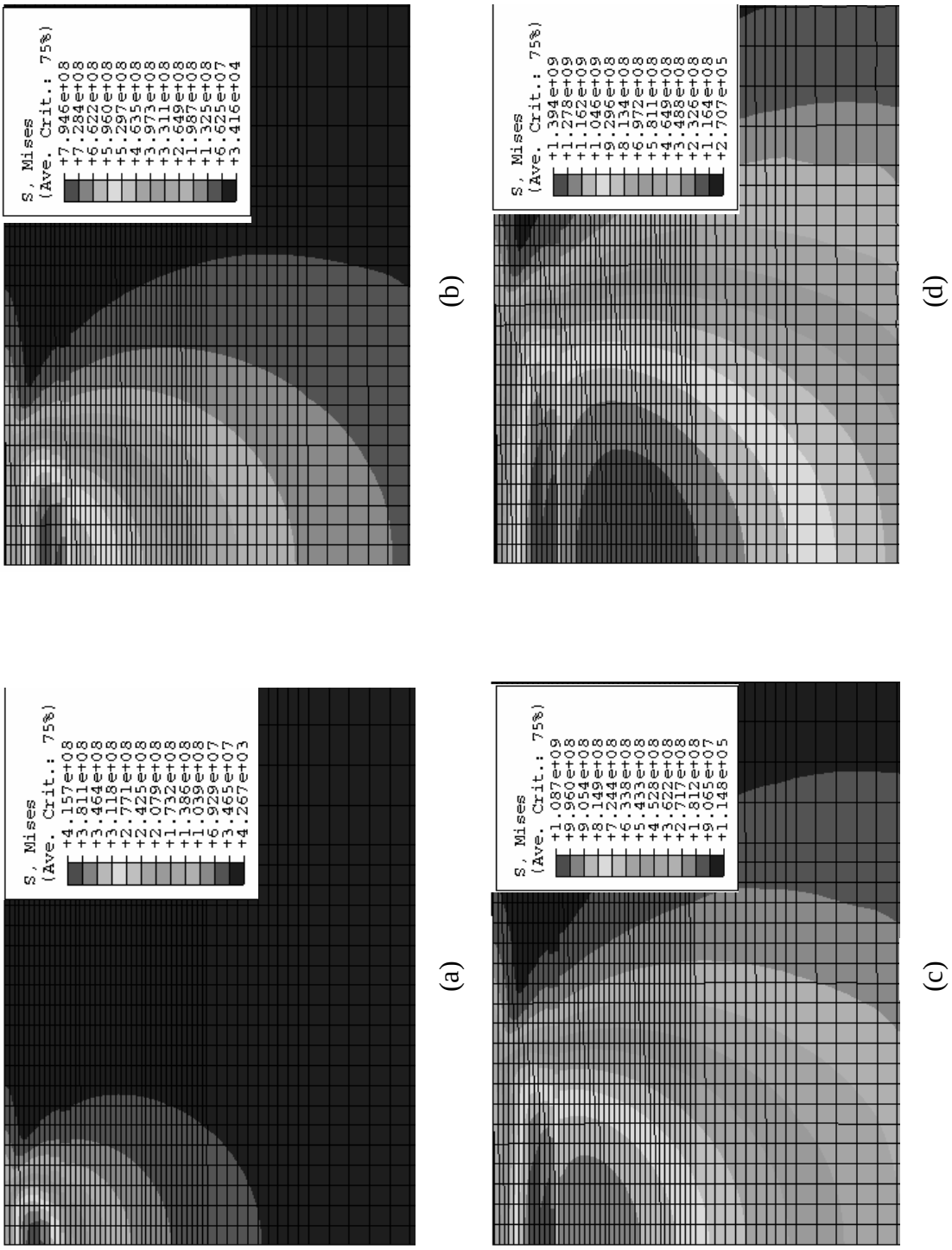

Figure 11. Contours of von Mises stress in layered and gradient coating system indented by a rigid spherical indenter for normal load; (a) W= 4.4×10^{-4} N, (b) 0.0035 N, (c) 0.0119 N, and (d) 0.0283 N

Figure 12 depicts the von Mises stress distribution on the plane of symmetry, X-Y plane, for 500nm $Ti_{.30}C_{.70}$ layer thickness, $W = 4.4 \times 10^{-4}$ N and $\mu = 0.0$. Figure 12(a) is the perspective view of the von Mises stress distribution generated below the contact surface along the axis of depth. It illustrates that the maximum von Mises stress with the magnitude of 0.408 GPa occurring inside the top $Ti_{.30}C_{.70}$ coating. Due to the discontinuous material properties at the coating interface, von Mises stress distribution displays drastic stress variations at the interface along the axis of depth. Figure 12(b) is the contour of von Mises stress distribution presented in Figure 12(a). Figure 13 shows the effect of top $Ti_{.30}C_{.70}$ coating thickness on von Mises stress for W = 0.0035 N and μ = 0.0. Depending on the top $Ti_{.30}C_{.70}$ coating thickness, the stress distributions along the axis of depth at the center of the contact vary significantly. With 100nm top $Ti_{.30}C_{.70}$ coating thickness, the maximum von Mises stress, 628 MPa, occurs at the $Ti_{.90}C_{.10}$ and α - Ti interface. As the top coating thickness increases to 400nm, the location of maximum von Mises stress, 818 MPa, moves to the $Ti_{.50}C_{.50}$ and $Ti_{.70}C_{.30}$ interface. When the top coating thickness is 700 nm, the maximum von Mises stress, 875 MPa, occurs at the $Ti_{.30}C_{.70}$ and $Ti_{.50}C_{.50}$ interface. Finally, when the 1000 nm thickness is used, the maximum von Mises stress, 813 MPa, occurs inside the top $Ti_{.30}C_{.70}$ coating. The thicker $Ti_{.30}C_{.70}$ coating (1000 nm) results in less magnitude of maximum von Mises stress than intermediate coatings thicknesses (400 nm and 700 nm). The results indicate that the maximum von Mises stress location can be moved vertically along the axis of depth depending on the coating thickness under the same normal load while the von Mises stress in the substrate changes negligibly. Also, the results suggest that the desirable top coating thickness changes depending on the loading conditions. Therefore the top layer thickness has a significant effect on the magnitude of the von Mises stress developed in the layered and gradient Ti/TiC coating system. It is noted that the maximum thickness of the top $Ti_{.30}C_{.70}$ layer is affected by the residual compressive stresses due to the thermal expansion coefficient differences.

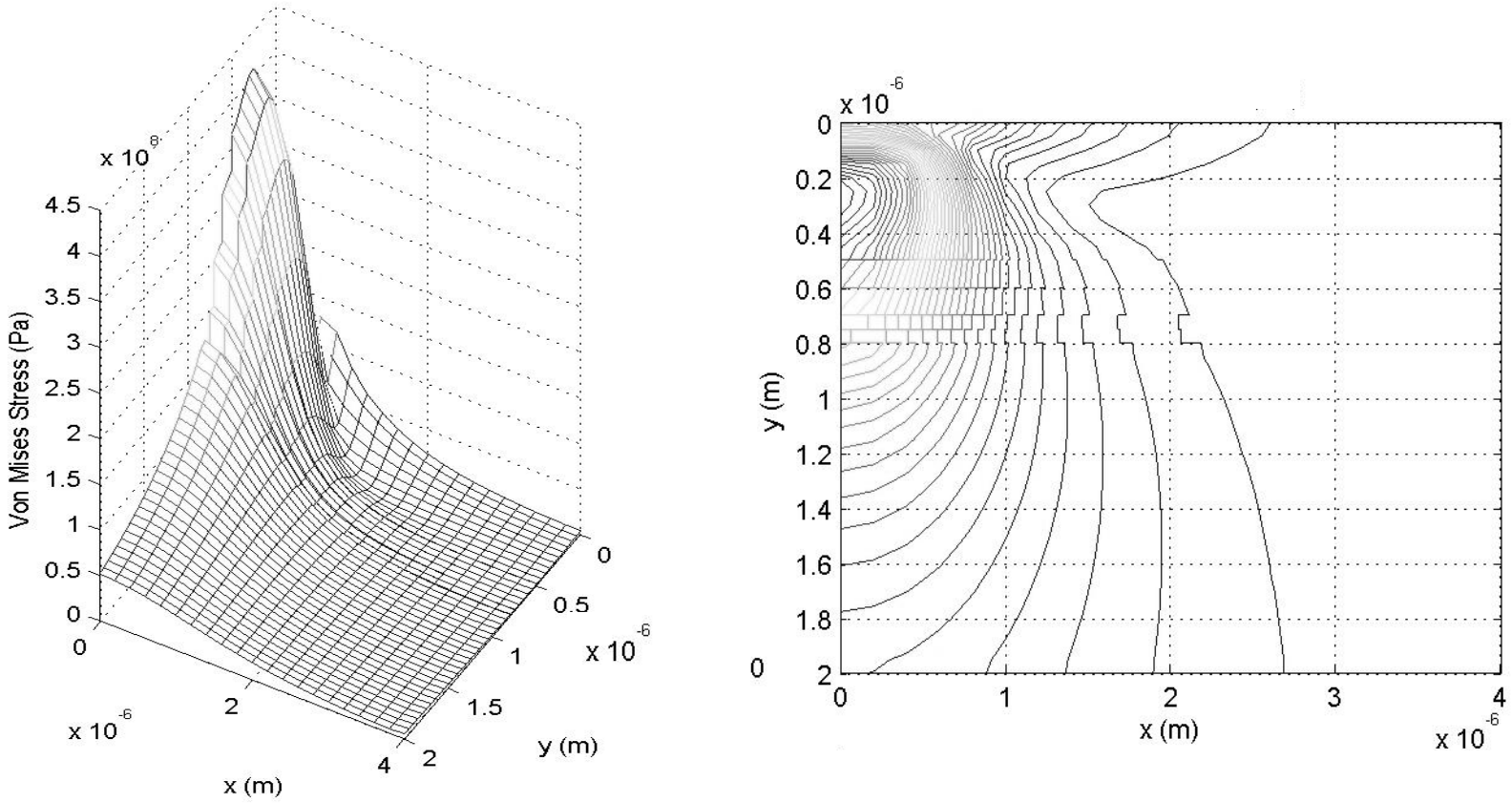

(a) (b)

Figure 12. Von Mises stress distribution in layered and gradient coating system indented by a rigid spherical indenter for $Ti_{.30}C_{.70}$ coating thickness, 500nm, normal load, 4.4×10^{-4} N, and friction coefficient, 0.0; (a) von Mises stress distribution and (b) contour of von Mises stress

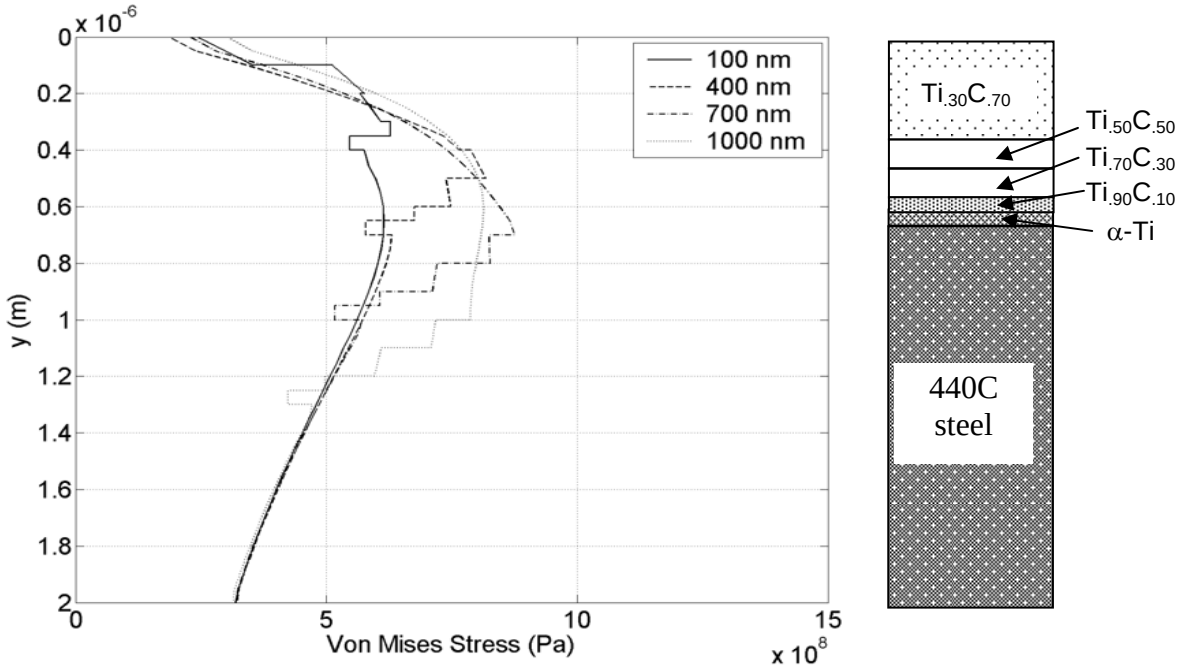

Figure 13. Effect of top $Ti_{.30}C_{.70}$ coating thickness on von Mises stress in layered and gradient coating system for various $Ti_{.30}C_{.70}$ thicknesses (W = 0.0035 and μ = 0.0)

Figure 14 depicts the effect of top coating thickness on contact pressure distribution indented by a rigid spherical indenter on the contact surface under W = 0.0035 N and μ = 0.0. The dashed line represents the pressure distribution generated on the semi-infinite medium without coatings. It illustrates the maximum Hertzian pressure, 1.0 GPa, is generated under the normal load, W = 0.0035 N. When the layered and gradient Ti/TiC coating system is applied, the maximum Hertzian pressure increases due to the stiffer coating layers. The dashpot line pressure distribution is generated for the 500nm top $Ti_{.30}C_{.70}$ layer thickness of layered and gradient Ti/TiC coating system. Due to the stiffer material properties of the coatings, the magnitude of maximum Hertzian pressure is higher with the narrower half contact width compared with the no layer Hertzian contact condition. The solid line pressure distribution is generated for the 1000nm top $Ti_{.30}C_{.70}$ layer thickness of layered and gradient Ti/TiC coating system. This line demonstrates highest magnitude of von Mises stress with the narrowest half contact width under the normal load, W = 0.0035 N. In general, the pressure magnitude increases due to not only the increase of Young's modulus but also the increase of top $Ti_{.30}C_{.70}$ coating thickness although the same normal load, W = 0.0035 N, is applied. In addition, the half Hertzian contact width decreases as the top coating thickness increases because the same magnitude of normal load is applied to the layered and gradient Ti/TiC coating system.

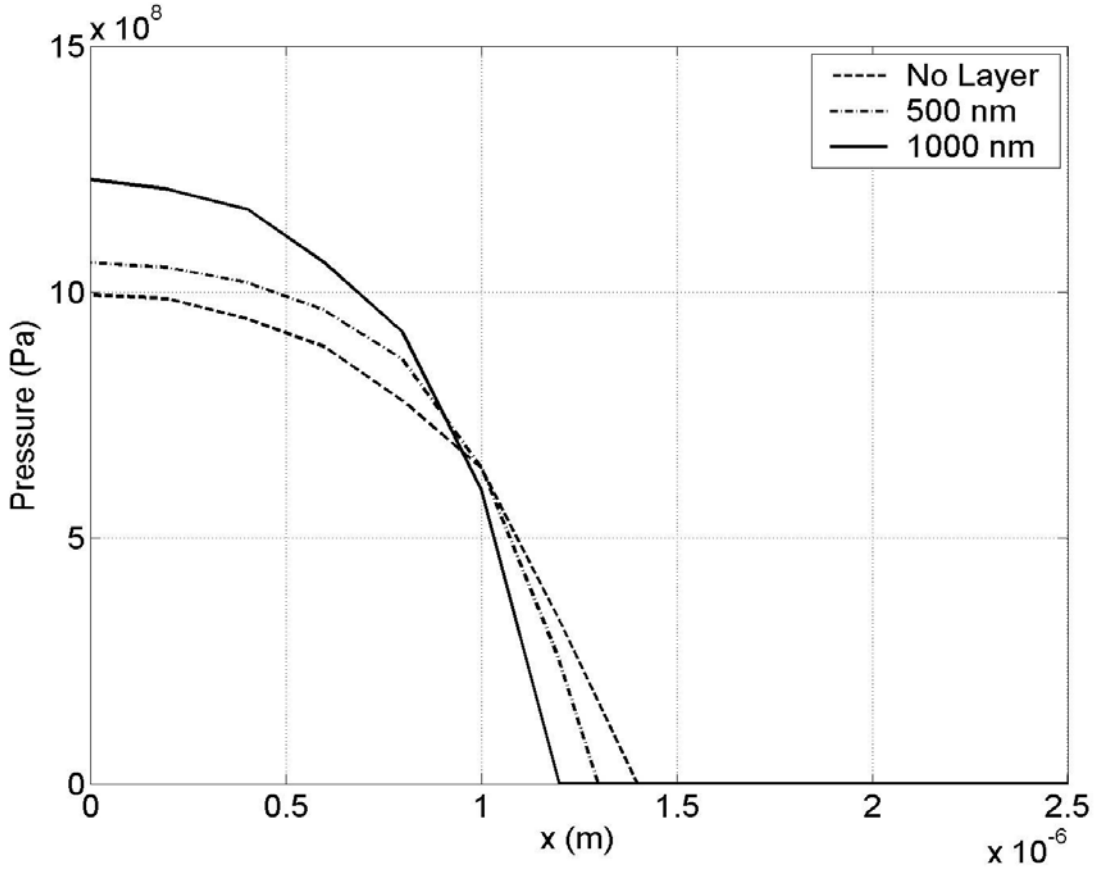

Figure 14. Effect of top coating thickness on contact pressure distribution on layered and gradient coating system indented by a rigid spherical indenter (W = 0.0035 N, μ = 0.0)

Figure 15 shows the effects of applied load on von Mises stress in layered and gradient Ti/TiC coating system indented by a rigid spherical indenter for various normal loads with 350nm $Ti_{.30}C_{.70}$ layer thickness and μ = 0.0. The magnitude of von Mises stress in the layered and gradient Ti/TiC coating system increases as the applied normal load increases from 0.0004N to 0.0283 N. The maximum von Mises stress for the normal load, W = 0.0004N, is 416 MPa occurring at the $Ti_{.30}C_{.70}$ and $Ti_{.50}C_{.50}$ interface. As the normal load increases, the magnitude and location of the maximum von Mises stress are changed. The maximum von Mises stress for the normal load, W = 0.0035 N, is 795 MPa occurring at the $Ti_{.50}C_{.50}$ and $Ti_{.70}C_{.30}$ interface. The maximum von Mises stress for the normal load, W = 0.0119 N, is 1.09 GPa at the $Ti_{.50}C_{.50}$ and $Ti_{.70}C_{.30}$ interface. Finally the maximum von Mises stress for the normal load, W = 0.0283 N, is 1.39 GPa at the $Ti_{.50}C_{.50}$ and $Ti_{.70}C_{.30}$ interface. Generally the magnitude and location of maximum von Mises stress distribution vary significantly depending on the magnitude of normal load when the layered and gradient Ti/TiC coating system is used.

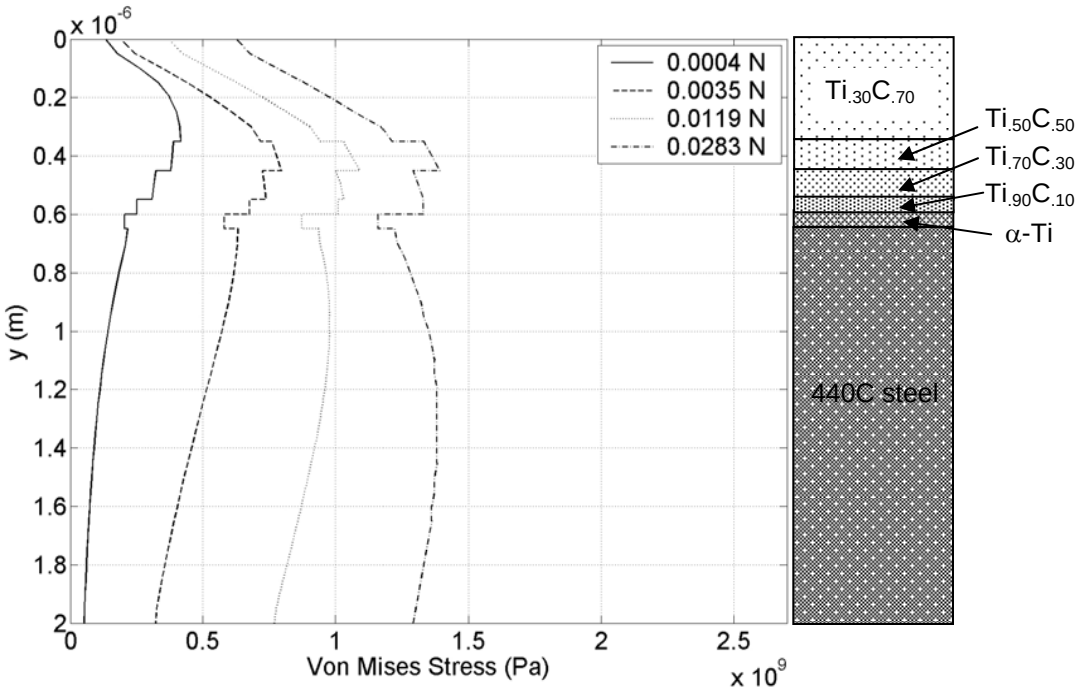

Figure 15. Effect of applied load on von Mises stress in layered and gradient coating system indented by a rigid spherical indenter for various normal loads ($Ti_{.30}C_{.70}$ = 350 nm, μ = 0.0)

Figure 16 depicts the effect of bond layer material on von Mises stress for W = 0.0035 N and μ = 0.0. Bond layer materials such as α-Ti, Ti alloy, and chromium are used. Table 2 contains the material properties such as modulus of elasticity and poisson's ratio for three bond layers. There are significant von Mises stress changes inside the bond layer. The higher the modulus of elasticity is, the higher the von Mises stress is. The negligible von Mises stress changes occur in the other coatings and substrate even if the substantial von Mises stress variation occurs in the bond layer. Using the stiffer bond layer like chromium increases the resistance to initiation of plastic deformation in the bond layer. However, it creates the higher von Mises stress differences at the interfaces above and below the bond layer.

In order to investigate the friction effect at the contact interface, the Coulomb friction was used at the rigid indenter and $Ti_{.30}C_{.70}$ coating interface. Figures 17 demonstrates the von Mises stress distribution generated in 350 nm $Ti_{.30}C_{.70}$ layer thickness coating system at the center of the contact along the axis of depth under the normal loading conditions for W = 4.4×10^{-4} N and W = 0.0283 N. Figure 17(a) illustrates that the effect of friction coefficient variation from μ = 0.0 to μ = 0.3 on von Mises stress variation near the surface is negligible under the low loading condition. The maximum von Mises stresses are produced at the $Ti_{.30}C_{.70}$ and $Ti_{.50}C_{.50}$ interface for μ = 0.0 through 0.3. At higher loading, W = 0.0283 N, there are significant von Mises stress distribution changes near the contact because the friction (tangential) force at the contact is proportional to applied load shown in Figure 17(b). Also, the magnitude of maximum von Mises stress increases

as the friction coefficients increase. However, the location of von Mises stress remains the same, at the $Ti_{.50}C_{.50}$ and $Ti_{.70}C_{.30}$ interface.

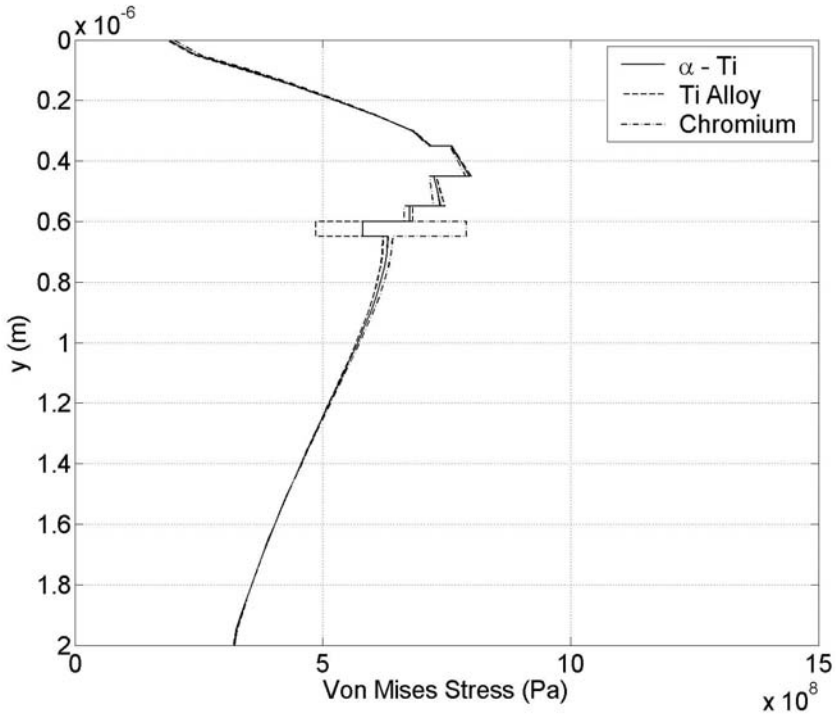

Figure 16. Effect of bond layer materials on von Mises stress in layered and gradient coating system for W = 0.0035 N and $\mu = 0.0$

	Modulus of Elasticity (GPa)	Poisson's Ratio
α - Ti	140	0.25
Ti Alloy	103	0.34
Chromium	279	0.21

Table 2. Material properties for bond layers

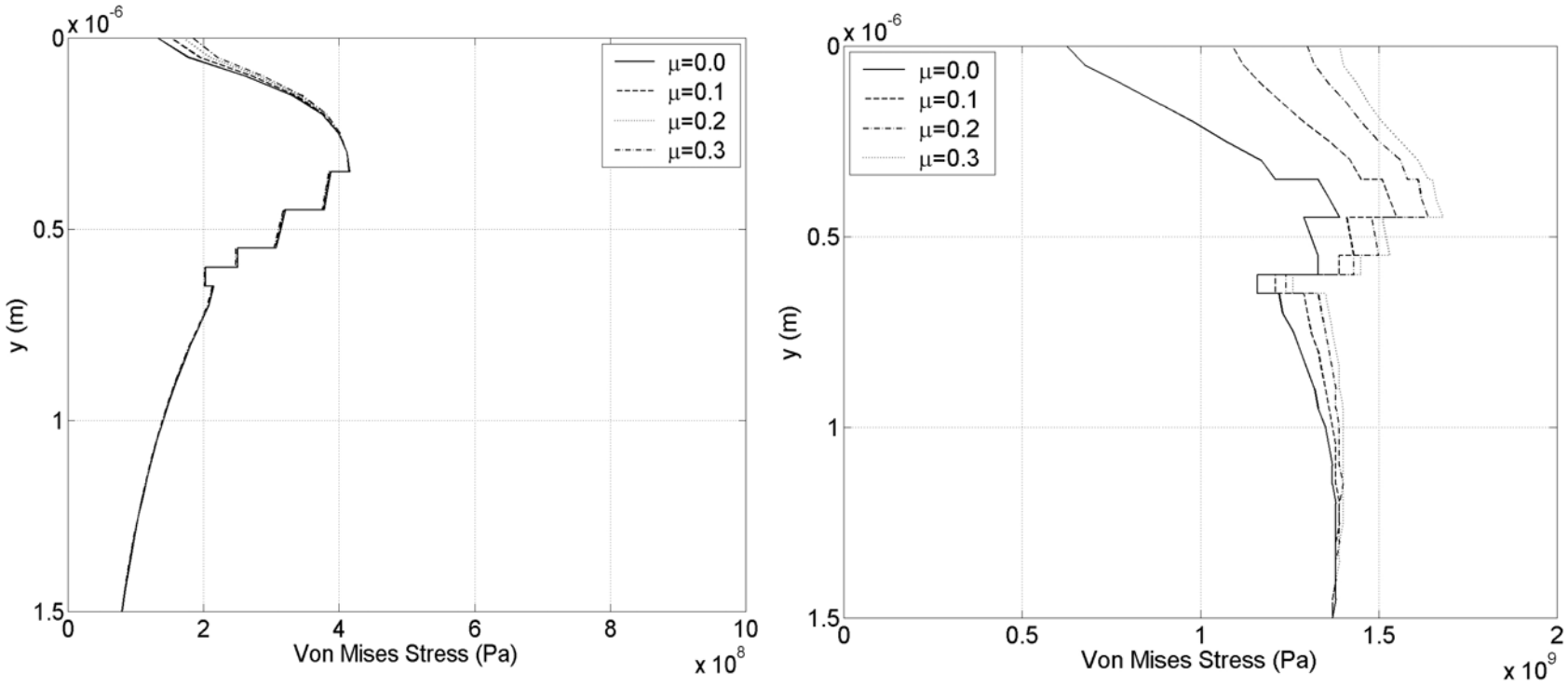

(a) (b)

Figure 17. Effect of friction coefficient on von Mises stress in layered and gradient coating system for normal load; (a) W = 4.4×10^{-4} N and (b) W = 0.0283 ($Ti_{.30}C_{.70}$ = 350 nm)

Figure 18 shows the effect of plasticity on von Mises stress for 350 nm $Ti_{.30}C_{.70}$ layer thickness, W = 0.15 N and $\mu = 0.0$. In order to obtain the yield strength of the materials used for the coating system, the following relationship is used because the strain-hardening is negligible for the coating materials used (Komvopolous, 1989).

$$\sigma_{yield} = \frac{hardness}{3}$$

Linear elastic-perfectly plastic stress-strain law was applied for the FEA model. Figure 18(a) demonstrates that the contour of von Mises stress indented by a rigid spherical indenter at the center of the contact. It depicts the high stress concentration inside the $Ti_{.50}C_{.50}$ layer. Also, it shows that the maximum von Mises stress occurs inside the substrate. Figure 18(b) illustrates von Mises stress at the center of contact along the axis of depth. Significant plastic deformation is developed inside the $Ti_{.30}C_{.70}$ and α-Ti coatings because the yield strength of the materials was reached as the normal load increases. Therefore, the plastic deformation of the coatings is initiated at the bond layer interface.

Plastic deformation is the major concern in design of the layered and gradient coating/substrate system because the tribological coating failure usually initiates and propagates from the plastic deformation zone.

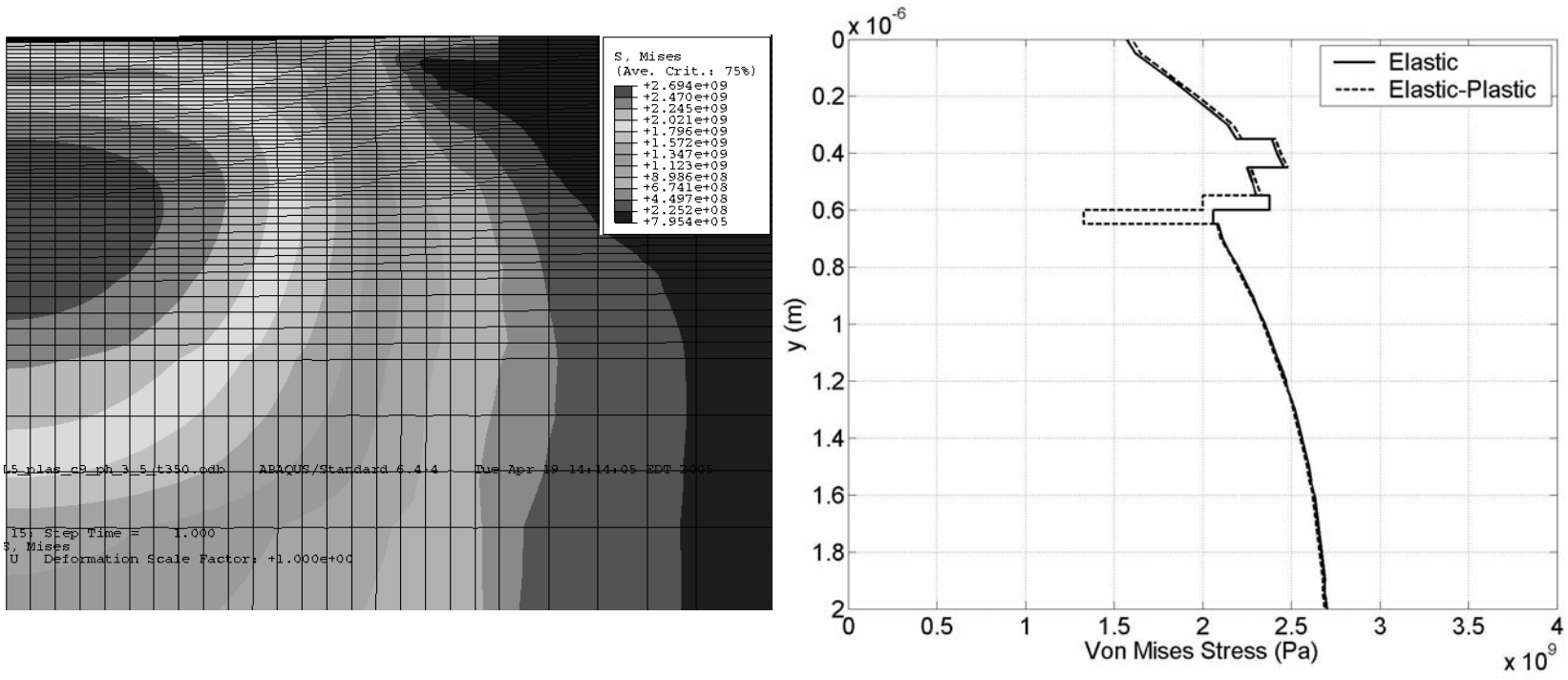

(a) (b)

Figure 18. Effect of plasticity on von Mises stress in layered and gradient coating system for $Ti_{.30}C_{.70}$ = 350 nm, W = 0.15 N, and μ = 0.0; (a) contour of von Mises stress on the plane of symmetry and (b) stress profile of von Mises stress along the centerline of the contact for elastic material properties and elastic-plastic material properties

Summary

Stress distributions in a layered and gradient TiC coating/440C steel substrate system indented by a rigid spherical indenter were determined using the finite element analysis model. Design superiority of the layered and gradient coating to monolayer coating was proved to improve the integrity of coating system. The layered and gradient Ti/TiC coatings generate smooth discrete stress transition at the coating interfaces when the chemistry and structure of the coating is varied. Therefore, the stress discontinuities at the interfaces are important design factor to consider. Top layer thickness is very influential to the layered and gradient Ti/TiC coating system because it changes the magnitude and location of maximum von Mises stress distribution inside the coating system significantly. Also, the top layer thickness changes the magnitude of maximum Hertzian pressure and half contact width under the same load condition due to the combination of the stiffness and thickness of the layer material. In addition, magnitude of the applied normal load affects the maximum Hertzian contact pressure and subsurface von Mises stress significantly. Effect of friction on subsurface von Mises stress is small for low loading conditions. However, effect of friction on subsurface von Mises stress is substantial for high loading conditions. Effect of the bond layer materials on the von Mises stress should be considered because yielding in the layered and gradient Ti/TiC coating system initiates at the bond layer when α-Ti bond layer is used.

In conclusion, stress distribution in the layered and gradient Ti/TiC coating system indented by a rigid spherical indenter depends strongly on many critical parameters such as the layer thicknesses, coating design, material properties, applied load, and the friction. Especially, the magnitude, location, and discontinuity of the von Mises stress at the interfaces play important roles on the interfacial failure of the coating system. Design of coating systems with layered and gradient Ti/TiC coatings increases the limitation of their applications when the loading conditions are specified.

Reference

(1) Bhattacharya, A. K. and Nix, W. D. (1988), “Analysis of Elastic and Plastic Deformation Associated with Indentation Testing of Thin Films on Substrates,” International Journal of Solids and Structures, Vol. 24, No. 12, pp. 1287-1298.

(2) Chiu, Y. P. and Hartnett, M. J. (1983), “A Numerical Solution for Layered Solid Contact Problems With Application to Bearings,” Journal of Lubrication Technology, Vol. 105, pp. 585-590.

(3) Chudoba, T., Schwartzer, N., and Richter, F. (2002), “Step Towards a Mechanical Modeling of Layered Systems”, Surface and Coatings Technology, Vol. 154, pp. 140-151.

(4) Cole, S. J. and Sayles, R. S. (1992), “A Numerical Model for the Contact of Layered Elastic Bodies With Real Rough Surfaces,” Journal of Tribology, Vol. 114, pp. 334-340.

(5) Gupta, P. K. and Walowit, J. A. (1974), “Contact Stresses Between an Elastic Cylinder and a Layered Elastic Solid,” ASME Journal of Lubrication Technology, Vol. 96, pp. 250-257.

(6) King, R. B. and O’Sullivan (1987), “Sliding Contact Stresses in a Two-Dimensional Layered Elastic Half-Space,” International Journal of Solids and Structures, Vol. 23, No. 5, pp. 581-597.

(7) Komvopulos, K. (1988), “Finite Element Analysis of a Layered Elastic Solid in Normal Contact With a Rigid Surface,” Journal of Tribology, Vol. 110, pp. 477-485.

Komvopulos, K. (1989), “Elastic-Plastic Finite Element Analysis of Indented Layered Media,” Journal of Tribology, Vol. 111, pp. 430-439.

(8) Kral, E. R. and Komvopoulos, K. (1997), “Three-Dimensional Finite Element Analysis of Subsurface Stress and Strain Fields Due to Sliding Contact on an Elastic-Plastic Layered Medium,” Journal of Tribology, Vol. 119, pp. 332-341.

(9) Kuo, C. H. and Keer, L. M. (1992), “Contact Stress Analysis of a Layered Transversely Isotropic Half-Space,” Journal of Tribology, Vol. 114, pp. 253-262.

(10) Meijers, P. (1968), “The Contact Problem of a Rigid Cylinder on an Elastic Layer,” Applied Scientific Research, Vol. 18, pp. 353-383.

(11) O’Sullivan, T. C. and King, R. B. (1988), “Sliding Contact Stress Field Due to a Spherical Indenter on a Layered Elastic Half-Space,” Journal of Tribology, Vol. 110, pp. 235-240.

(12) Polonsky, I. A. and Keer, L. M. (2000), “A Fast and Accurate Method for Numerical Analysis of Elastic Layered Contacts”, Journal of Tribology, Vol. 122, pp. 30-35.

(13) Sun, Y, Bloyce, A., and Bell, T. (1995), “Finite element analysis of plastic deformation of various TiN coating/substrate systems under normal contact with a rigid sphere,” Thin Solid Films, Vol. 271, pp. 122-131.

(14) Voevodin, A. A., Donley, M. S., Zabinski, J. S. and Bultman, J. E. (1995), "Mechanical and Tribological Properties of Diamond-like Carbon Coatings Prepared by Pulsed Laser Deposition," Surface and Coatings Technology, Vol. 76-77, pp. 534-539.

(15) Voevodin, A. A., Walck, S. D. and Zabinski, J. S. (1997a), "Architecture of Multilayer Nanocomposite Coatings with Super-Hard Diamond-like Carbon Layers for Wear Protection at High Contact Loads," Wear, Vol. 203-204, pp. 516-527.

(16) Voevodin, A. A., Capano, M. A., Laube, S. J. P., Donley, M. S. and Zabinski, J. S. (1997b), "Design of a Ti/TiC/DLC functionally gradient coating based on studies of structural transitions in Ti-C thin films," Thin Solid Films, Vol. 298, pp. 107-115.

(17) Ye, N. and Komvopoulos, K. (2003), "Effect of Residual Stress in Surface Layer on Contact Deformation of Elastic-Plastic Layered Media," Journal of Tribology, Vol. 125, pp. 692-699.